OXFORD CDE

Journal of Computational Design and Engineering, 2020, 0(0), 1–15

doi: 10.1093/jcde/qwaa051
Journal homepage: www.jcde.org

RESEARCH ARTICLE

Stability analysis of nanobeams in hygrothermal environment based on a nonlocal strain gradient Timoshenko beam model under nonlinear thermal field

Subrat Kumar Jena[1], S. Chakraverty[1,*] and Mohammad Malikan[2]

[1]Department of Mathematics, National Institute of Technology Rourkela, Rourkela, Odisha 769008, India and
[2]Department of Mechanics of Materials and Structures, Faculty of Civil and Environmental Engineering, Gdansk University of Technology, Gdansk, 80-233 Poland

*Corresponding author. E-mail: sne.chak@yahoo.com http://orcid.org/0000-0003-4857-644X

Abstract

This article is dedicated to analyzing the buckling behavior of nanobeam subjected to hygrothermal environments based on the principle of the Timoshenko beam theory. The hygroscopic environment has been considered as a linear stress field model, while the thermal environment is assumed to be a nonlinear stress field based on the Murnaghan model. The size-dependent effect of the nanobeam is captured by the nonlocal strain gradient theory (NSGT), and the governing equations of the proposed model have been derived by implementing a variational principle. The critical buckling loads have been calculated for the hinged–hinged boundary condition by incorporating the Navier approach and considering other elasticity theories such as classical elasticity theory, Eringen nonlocal elasticity theory, and strain gradient theory along with the NSGT. The present model is also validated with the pre-existing model in exceptional cases. Further, a parametric investigation has been performed to report the influence of various scaling parameters like hygroscopic environment, thermal environment, length-to-diameter ratio, small scale parameter, and length scale parameter on critical buckling loads by considering both the linear and nonlinear temperature distributions.

Keywords: hygrothermal environment; stability analysis; nonlinear temperature distribution; Timoshenko beam theory; nonlocal strain gradient model

1. Introduction

The advent of nanotechnology and the increasing demand for advanced equipment have led to the development of microelectromechanical and nanoelectromechanical systems. Some industrial equipment requires tiny and precise nanoscale displacements. Given that industrial actuators have a fast and accurate response and are highly durable, this can be a good solution to meet this need. In many industries, mainly in the automotive and the medical industries (Ikeda et al., 1990; Fatikow & Rembold, 1997), industrial actuators are commonly used in the form of nanobeams.

Structural designers are always aware of the fact that the loading, in terms of thermal loads applied to the structure, is more complex than other forms of loads such as gravity and mechanical loads. Generally, when a structural element is affected by tem-

Received: 24 February 2020; **Revised:** 28 April 2020; **Accepted:** 10 May 2020

perature changes, it tends to deform and, if it is restricted, it develops an internal force within the element. On the contrary, if the element is allowed to deform freely, no internal force is created in the element. For example, when a beam with complete freedom of movement is heated uniformly, its length will increase. If the same beam is heated with two-stranded ends, e.g. hinged–hinged (HH) support, there will be a transverse deformation and compressive force. This compressive force can have a direct effect on the mechanical deformation of the element. Therefore, nanobeams, as a vital part of NEMS, should be considered under both the linear and nonlinear distributions of temperature. That is why the authors were motivated to work on this theoretical research. In the case of nanobeams, we may found numerous published papers. For example, in terms of buckling or stability of nanobeams, researchers and engineers have conducted lots of studies (Wang, Zhang, Ramesh, & Kitipornchai, 2006; Ansari, Sahmani, & Rouhi, 2011a,b; Pradhan & Reddy, 2011; Roque, Ferreira, & Reddy, 2011; Pradhan, 2012; Akgöz & Civalek, 2017; She, Yuan, Ren, & Xiao, 2017; Eltaher, Kabeel, Almitani, & Abdraboh, 2018; Jena & Chakraverty, 2019a; Jena, Chakraverty, Jena, & Tornabene, 2019; Jena, Chakraverty, & Malikan, 2019; Jena, Chakraverty, & Tornabene, 2019a; Malikan, 2019). Likewise, one can find some valuable existing literature (Zhen & Fang, 2010; Ebrahimi & Barati, 2017a,b; Malikan, Nguyen, & Tornabene, 2018; Barati, Faleh, & Zenkour, 2019; Jena, Chakraverty, Malikan, & Tornabene, 2019; She, Jiang, & Karami, 2019; Karami, Janghorban, & Rabczuk, 2020) concerning thermal influences. Arefi and Zenkour studied bending, and vibration of three-layered geometrically irregular (Arefi & Zenkour, 2017a) and straight (Arefi & Zenkour, 2017b) nanoscale piezomagnetic beams, large deflections of a functionally graded (FG) laminated nanosize beam under thermomagnetic field (Arefi & Zenkour, 2016) and developed static investigations on the curved nanobeams with respect to electromagnetic effects (Arefi & Zenkour, 2019a). In their works, to gain shear deformations benefits, a sinusoidal shear deformation theory was utilized. Moreover, Arefi and Soltan Arani (2018) conducted a thermoelastic analysis to capture the results for large deflections for a nonlocal beam exposed in thermal, magnetic, and electric stress fields. Sometimes in the analysis of beam materials, there is no information about mechanical properties or on the other side sometimes there are some imperfect characteristics that make the material properties of beams uncertain about using exactly at a constant value. It arises in observable physical measurements as some research about nanobeams can be seen in this category (Vu-Bac, Lahmer, Zhuang, Nguyen-Thoi, & Rabczuk, 2016; Jena, Chakraverty, & Malikan, 2020a). As most of the research work on the nanostructures is in the framework of differential equations, hence it is crucial to understand a better concept to solve these equations (Anitescu, Atroshchenko, Alajlan, & Rabczuk, 2019; Rabczuk, Ren, & Zhuang, 2019; Samaniego et al., 2020). As per the limited knowledge of the authors, there is no recorded paper or a little work about the nonlinear distribution of temperature for the stability analysis nanobeam available. Some other works related to micro/nanostructures can be found in different researches (Arefi & Zenkour, 2017c, 2018a, 2018b, 2019b; Arefi, Bidgoli, & Zenkour, 2018; Jena & Chakraverty, 2018; Jena, Chakraverty, & Jena, 2019; Jena & Chakraverty, 2019b,c; Jena, Chakraverty, & Tornabene, 2019b; Malikan, 2020; Malikan, Krasheninnikov, & Eremeyev, 2020; Sedighi & Malikan, 2020; Sedighi, Ouakad, Dimitri, & Tornabene, 2020; Senthilkumar, 2020; Vinyas, Harursampath, & Kattimani, 2020; Malikan & Eremeyev, 2020a).

For the sake of brevity, we have only considered the closest research to the ongoing work in detail. Ebrahimi and Salari (2015) studied the dynamic characteristics of the functionally graded nanobeams by considering the thermal environment as a linear function and calculated the natural frequencies and stability capacity of the beam. Also, the stress nonlocality was adopted to model the low-scale impacts. Mohammadi, Safarabadi, Rastgoo, and Farajpour (2016) investigated the vibration behavior of the rotating viscoelastic nanobeam, which was embedded in a visco-Pasternak elastic foundation subjected to the effects of humidity as well as the thermal environment. Moreover, the thermal environment was assumed as the nonlinear thermal stress field on the basis of the Murnaghan assumption. The differential quadrature method was utilized to solve the equations that were derived based on the Euler–Bernoulli beam. Jouneghani, Dimitri, and Tornabene (2018) proposed a model considering the porous functionally graded nanobeams with hygroscopic and thermal loadings. They also used the Eringen nonlocal model in conjunction with the Timoshenko beam theory. Navier's solution technique helped them to solve the harvested mathematical relations.

Based on the Timoshenko beam theory, this paper explores the stability response of nanobeam subjected to hygrothermal conditions. The temperature distribution is assumed to be changed nonlinearly along with the thickness following the Murnaghan model, while the hygroscopic environment is assumed linearly. The size-dependent behavior of the nanobeam is examined by incorporating the nonlocal strain gradient hypothesis. The required stability equations are derived based on the variational principle and nonlinear Lagrangian strains. Navier's approach is employed to compute the critical buckling loads of the nanobeam for the HH boundary condition. As far as we have confronted with different size-dependent theories, this paper presents the results not only for NSGT but also in a full comparison with other small-scale models, i.e. Eringen Nonlocal Elasticity Theory (ENET), and Strain Gradient Theory (SGT) along with the NSGT. The current model is also verified with well-known literature. Consequently, a full parametric study is presented based on the different key and vital parameters, e.g. nonlinear thermal surrounding, hygroscopic environment, length-to-diameter ratio, small scale parameter, and strain gradient length scale parameter on critical buckling loads.

2. Proposed Model

In this study, a nanobeam of length L, and diameter d has been taken into the investigation, which is exposed to a linear hygroscopic environment and nonlinear thermal environment based on the Murnaghan model. The schematic diagram of this model is illustrated in Fig. 1. In the forthcoming subsection, reviews of nonlocal strain gradient theory and hygrothermal environments have been abridged, and the governing equations for the proposed model have been derived.

2.1. Review of the nonlocal strain gradient theory

Total stress field tensor, as per the nonlocal strain gradient theory (Lim, Zhang, & Reddy, 2015; Li & Hu, 2016; Lu, Guo, & Zhao, 2017; Malikan & Nguyen, 2018; Malikan, Dimitri, & Tornabene, 2018; Jena, Chakraverty, & Tornabene, 2019c; Malikan & Eremeyev, 2020b),

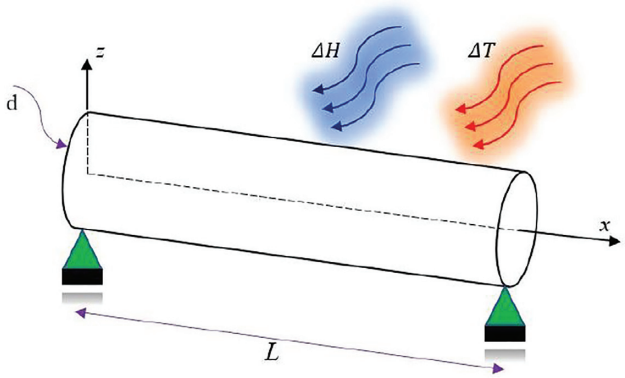

Figure 1: Schematic diagram of a nanobeam subjected to hygrothermal environments.

depends on not only classical nonlocal stress tensor but also higher order nonlocal stress tensor that is presented as

$$t = \sigma - \nabla\sigma^{\bullet}, \tag{1}$$

where $\sigma = \int_0^L E\alpha(x, x', e_0a)\,\varepsilon'_{xx}(x')\,dx'$ and $\sigma^{\bullet} = l^2\int_0^L E\alpha^*(x, x', e_1a)\,\varepsilon'_{xx,x}(x')\,dx'$ are the classical nonlocal stress tensor and the higher order nonlocal stress tensor, respectively. $\alpha(x, x', e_0a)$ and $\alpha^*(x, x', e_1a)$ represent the nonlocal kernels, ε_{xx} and $\varepsilon_{xx,x}$ represent the component of strain tensor and gradient of the strain tensor, L and l denote the external characteristics—length of the beam and material length scale parameter, and e_0a and e_1a are the nonlocal parameters due to the lower order and higher order strain gradient stress fields. Applying the nonlocal differential operator ($\ell_i = 1 - (e_ia)^2\nabla^2$, $i = 0, 1$) on the stress field defined in Equation (1), we obtain

$$\left(1 - (e_0a)^2\nabla^2\right)\left(1 - (e_1a)^2\nabla^2\right)\sigma_{xx} = E\left(1 - (e_1a)^2\nabla^2\right)\varepsilon_{xx} - El^2\left(1 - (e_0a)^2\nabla^2\right)\nabla^2\varepsilon_{xx} \tag{2}$$

in which Laplacian is denoted by ∇^2, E presents elastic modulus, σ_{xx} exhibits nonlocal axial stress, and ε_{xx} demonstrates local axial strain. Assuming $e_0a = e_1a$, the first-order nonlocal strain gradient model for 1D elastic material will be modified as

$$\left(1 - (e_0a)^2\frac{\partial^2}{\partial x^2}\right)\sigma_{xx} = E\left(1 - l^2\frac{\partial^2}{\partial x^2}\right)\varepsilon_{xx}. \tag{3}$$

2.2. Review of hygrothermal environment

Based on thermal elasticity theory, the axial force due to the thermal environment (N^T) can be given as (Je̜kot, 1996; Mohammadi, Safarabadi, Rastgoo, & Farajpour, 2016; Takahashi, 2018)

$$N^T = -\int_A \Phi(\Delta T)\,dA \tag{4}$$

in which $\Phi(\Delta T)$ is the nonlinear elastic stress temperature coefficient, which may be defined as (Je̜kot, 1996; Mohammadi, Safarabadi, Rastgoo, & Farajpour, 2016; Takahashi, 2018)

$$\Phi(\Delta T) = E\alpha_x\Delta T - \hat{h}\alpha_x^2\Delta T^2 \quad \text{with} \quad \hat{h} = l_1(1 - 2\upsilon) - 2m_1(\upsilon^2 - 1) + n_1\upsilon^2, \tag{5}$$

where ΔT is the change in temperature, α_x is the coefficient of thermal expansion, (l_1, m_1, n_1) are Murnaghan's third-order elastic constants, and υ is Poisson's ratio.

Substituting Equation (5) into Equation (4), we obtain

$$N^T = -\int_A \Phi(\Delta T)\,dA = -\int_A \left(E\alpha_x\Delta T - \hat{h}\alpha_x^2\Delta T^2\right)dA = -\left(EA\alpha_x\Delta T - A\hat{h}\alpha_x^2\Delta T^2\right). \tag{6}$$

According to hygroscopic elasticity theory, the axial force due to the hygroscopic environment (N^H) can be presented as (Je̜kot, 1996; Mohammadi, Safarabadi, Rastgoo, & Farajpour, 2016; Takahashi, 2018)

$$N^H = -\int_A \varphi(\Delta H)\,dA. \tag{7}$$

Here, $\varphi(\Delta H)$ is the elastic stress due to hygroscopic environment, which is defined as

$$\varphi(\Delta H) = E\beta_x\Delta H \tag{8}$$

in which β_x denotes the hygroscopic expansion coefficient, and ΔH is the change in moisture concentration.

Plugging Equation (8) into Equation (7), we have

$$N^H = -\int_A \varphi(\Delta H)\,dA = -\int_A (E\beta_x\Delta H)\,dA = -EA\beta_x\Delta H. \tag{9}$$

2.3. A mathematical formulation of the proposed model

The displacement field, as per Timoshenko beam theory, is stated as (Wang, Zhang, Ramesh, & Kitipornchai, 2006; Reddy, 2007)

$$u_1(x, z, t) = u(x, t) + z\varphi(x, t) \tag{10.a}$$

$$u_2(x, z, t) = 0 \tag{10.b}$$

$$u_3(x, z, t) = w(x, t) \tag{10.c}$$

in which $u(x, t)$ is the axial displacement of in-plane, $w(x, t)$ is the transverse displacement of middle-plane, u_i $(i = 1, 3)$ are the axial and transverse displacements of beam nodes, and $\varphi(x, t)$ denotes the rotation of beam nodes.

Using von Kármán nonlinear strain–displacement relationship, the Lagrangian strain may be obtained as

$$\varepsilon_{xx} = \frac{\partial u}{\partial x} + z\frac{\partial \varphi}{\partial x}, \tag{11.a}$$

$$\gamma_{xz} = \varphi + \frac{\partial w}{\partial x}. \tag{11.b}$$

Here, ε_{xx} represents the normal strain and γ_{xz} denotes the transverse shear strain. Considering the axial strain due to hygrothermal environments, Equation (11) will be converted into

$$\varepsilon_{xx} = \frac{\partial u}{\partial x} + z\frac{\partial \varphi}{\partial x} - \left(\alpha_x \Delta T - \frac{\hat{h}\alpha_x^2 \Delta T^2}{E}\right) - \beta_x \Delta H. \tag{12.a}$$

$$\gamma_{xz} = \varphi + \frac{\partial w}{\partial x}. \tag{12.b}$$

To further clarify, Equation (12.a) is mechanical strain relation equaling to total strain minus both strains resulted from thermal environment $(\alpha_x \Delta T - \frac{\hat{h}\alpha_x^2 \Delta T^2}{E})$ and strain originated from hygroscopic influence $(\beta_x \Delta H)$. If we remove the hygrothermal effects, the total strain would be equal to mechanical strain.

Taking variation in strain energy, the virtual strain energy δU is presented as

$$\begin{aligned}
\delta U &= \iiint_V \left(\sigma_{xx}\delta\varepsilon_{xx} + \sigma_{xx}^{(1)}\nabla\delta\varepsilon_{xx} + \sigma_{xz}\delta\gamma_{xz} + \sigma_{xz}^{(1)}\nabla\delta\gamma_{xz}\right) dV \\
&= \iiint_V \left[\left(\sigma_{xx} - \nabla\sigma_{xx}^{(1)}\right)\delta\varepsilon_{xx} + \left(\sigma_{xz} - \nabla\sigma_{xz}^{(1)}\right)\delta\gamma_{xz}\right] dV \\
&= \iiint_V \left[\begin{array}{l}\left(\sigma_{xx} - \nabla\sigma_{xx}^{(1)}\right)\delta\left(\dfrac{\partial u}{\partial x} + z\dfrac{\partial \varphi}{\partial x} - \left(\alpha_x \Delta T - \dfrac{\hat{h}\alpha_x^2 \Delta T^2}{E}\right) - \beta_x \Delta H\right) \\ + \left(\sigma_{xz} - \nabla\sigma_{xz}^{(1)}\right)\delta\left(\varphi + \dfrac{\partial w}{\partial x}\right)\end{array}\right] dV \\
&= \int_0^L \left[N_{xx}\frac{\partial \delta u}{\partial x} + M_{xx}\frac{\partial \delta \varphi}{\partial x} + Q_{xz}\left(\delta\varphi + \frac{\partial \delta w}{\partial x}\right)\right] dx \\
&= \int_0^L \left[-\frac{\partial N_{xx}}{\partial x}\delta u - \frac{\partial M_{xx}}{\partial x}\delta\varphi + Q_{xz}\delta\varphi - \frac{\partial Q_{xz}}{\partial x}\delta w\right] dx
\end{aligned} \tag{13}$$

in which $M_{xx} = \int_A z(\sigma_{xx} - \nabla\sigma_{xx}^{(1)})dA$, $N_{xx} = \int_A (\sigma_{xx} - \nabla\sigma_{xx}^{(1)})dA$, and $Q_{xz} = \int_A (\sigma_{xz} - \nabla\sigma_{xz}^{(1)})dA$ are the local stress resultants of the beam.

The virtual work done (δW) by external loads such as nonlinear thermal environment, and the hygroscopic environment as well as mechanical compressive loads, is obtained as

$$\delta W = -\int_0^L \left[-(E A\beta_x \Delta H)\left(\frac{\partial^2 w}{\partial x^2}\right) - \left(E A\alpha_x \Delta T - A\hat{h}\alpha_x^2 \Delta T^2\right)\left(\frac{\partial^2 w}{\partial x^2}\right) - N_{xx}^0\left(\frac{\partial^2 w}{\partial x^2}\right)\right]\delta w dx, \tag{14}$$

where N_{xx}^0 is the axial compressive force. Employing the variational principle and collecting the coefficients of δu, δw, $\delta\varphi$, we have

$$\frac{\partial N_{xx}}{\partial x} = 0, \tag{15.a}$$

$$\frac{\partial Q_{xz}}{\partial x} - N_{xx}^0\frac{\partial^2 w}{\partial x^2} - (E A\beta_x \Delta H)\left(\frac{\partial^2 w}{\partial x^2}\right) - \left(E A\alpha_x \Delta T - A\hat{h}\alpha_x^2 \Delta T^2\right)\left(\frac{\partial^2 w}{\partial x^2}\right) = 0, \tag{15.b}$$

$$\frac{\partial M_{xx}}{\partial x} - Q_{xz} = 0. \tag{15.c}$$

From the Hookean stress–strain elasticity relation for the Timoshenko beam theory based on Equation (12), we have

$$M_{xx} = E I\frac{\partial \varphi}{\partial x}, \tag{16.a}$$

$$Q_{xz} = k_s AG\left(\varphi + \frac{\partial w}{\partial x}\right), \tag{16.b}$$

where G is the shear modulus, A is the cross-section area, k_s is the shear correction factor, and $I = \int_A z^2 dA$ is the second area moment of inertia.

From the nonlocal strain gradient theory, i.e. from Equation (3), we have

$$\left(1 - (e_0 a)^2\frac{\partial^2}{\partial x^2}\right)\sigma_{ij} = C_{ijkl}\left(1 - l^2\frac{\partial^2}{\partial x^2}\right)\varepsilon_{kl} \tag{17}$$

in which σ_{ij}, ε_{kl}, and C_{ijkl} are stress tensor, strain tensor, and elastic modulus constant, respectively.

In this study, the size-dependent effect has been incorporated into normal stress and strain, whereas no size-dependent effect is injected into the constitutive relation of shear stress or strain. Therefore, from Equations (16) and (17), the nonlocal stress resultants may be obtained as

$$\left(1-(e_0a)^2\frac{\partial^2}{\partial x^2}\right)M_{xx}=EI\left(\frac{\partial\varphi}{\partial x}-l^2\frac{\partial^3\varphi}{\partial x^3}\right), \tag{18.a}$$

$$Q_{xz}=k_sAG\left(\varphi+\frac{\partial w}{\partial x}\right). \tag{18.b}$$

Now, using Equations (15) and (18), the governing equations for the proposed model may be stated as

$$k_sAG\left(\frac{\partial\varphi}{\partial x}+\frac{\partial^2 w}{\partial x^2}\right)-N^0_{xx}\frac{\partial^2 w}{\partial x^2}-(EA\beta_x\Delta H)\left(\frac{\partial^2 w}{\partial x^2}\right)-\left(EA\alpha_x\Delta T-A\hat{h}\alpha_x^2\Delta T^2\right)\left(\frac{\partial^2 w}{\partial x^2}\right)=0, \tag{19.a}$$

$$k_sAG\left(\varphi+\frac{\partial w}{\partial x}\right)+(e_0a)^2\frac{\partial}{\partial x}\left[\begin{matrix}-N^0_{xx}\frac{\partial^2 w}{\partial x^2}-(EA\beta_x\Delta H)\left(\frac{\partial^2 w}{\partial x^2}\right)-\\ \left(EA\alpha_x\Delta T-A\hat{h}\alpha_x^2\Delta T^2\right)\left(\frac{\partial^2 w}{\partial x^2}\right)\end{matrix}\right]-EI\frac{\partial}{\partial x}\left(\frac{\partial\varphi}{\partial x}-l^2\frac{\partial^3\varphi}{\partial x^3}\right)=0. \tag{19.b}$$

Putting $N^0_{xx}=P$ in Equation (19), where P is the applied compressive force due to mechanical load, we will have

$$k_sAG\left(\varphi+\frac{\partial w}{\partial x}\right)+(e_0a)^2\left[\begin{matrix}-P-(EA\beta_x\Delta H)-\\ \left(EA\alpha_x\Delta T-A\hat{h}\alpha_x^2\Delta T^2\right)\end{matrix}\right]\left(\frac{\partial^3 w}{\partial x^3}\right)-EI\left(\frac{\partial^2\varphi}{\partial x^2}-l^2\frac{\partial^4\varphi}{\partial x^4}\right)=0, \tag{20.a}$$

$$k_sAG\left(\frac{\partial\varphi}{\partial x}+\frac{\partial^2 w}{\partial x^2}\right)-P\frac{\partial^2 w}{\partial x^2}-(EA\beta_x\Delta H)\left(\frac{\partial^2 w}{\partial x^2}\right)-\left(EA\alpha_x\Delta T-A\hat{h}\alpha_x^2\Delta T^2\right)\left(\frac{\partial^2 w}{\partial x^2}\right)=0. \tag{20.b}$$

3. An Analytical Solution to the Proposed Model

In this study, Navier's method has been employed to solve the hygromechanical stability equation of Timoshenko nanobeam for HH boundary condition considering the nonlinear temperature distribution environment. The transverse displacement $w(x,\,t)$ and the rotation of cross-section $\varphi(x,\,t)$ are given as (Malikan, Dimitri, & Tornabene, 2019; Jena, Chakraverty, Malikan, & Tornabene, 2020; Jena, Chakraverty, Malikan, & Sedighi, 2020a, b; Jena, Chakraverty, & Malikan, 2020b,c)

$$w\,(x,\,t)=\sum_{m=1}^{\infty}W_m\sin\left(\frac{n\pi}{L}x\right), \tag{21}$$

$$\varphi\,(x,\,t)=\sum_{m=1}^{\infty}\Phi_m\cos\left(\frac{n\pi}{L}x\right), \tag{22}$$

in which W_m and Φ_m are the amplitudes of transverse displacement and rotation of cross-section, respectively. Substituting Equations (21) and (22) into Equation (20) yields

$$\left[\begin{matrix}k_sAG\left(\frac{n\pi}{L}\right)-(e_0a)^2\left[\left(\begin{matrix}-P-EA\beta_x\Delta H-\\ EA\alpha_x\Delta T+A\hat{h}\alpha_x^2\Delta T^2\end{matrix}\right)\left(\frac{n\pi}{L}\right)^3\right] & k_sAG+EI\left(\frac{n\pi}{L}\right)^2\left[1+l^2\left(\frac{n\pi}{L}\right)^2\right]\\ k_sAG\left(\frac{n\pi}{L}\right)^2+\left[\left(\begin{matrix}-P-EA\beta_x\Delta H-\\ EA\alpha_x\Delta T+A\hat{h}\alpha_x^2\Delta T^2\end{matrix}\right)\left(\frac{n\pi}{L}\right)^2\right] & k_sAG\left(\frac{n\pi}{L}\right)\end{matrix}\right]\left[\begin{matrix}W_m\\ \Phi_m\end{matrix}\right]=0. \tag{23}$$

Taking determinant of the above matrix, the buckling loads of the proposed system can be found out. Substituting $n=1$ yields critical buckling loads (P_{cr}) of the proposed model. From Equation (23), we may also get the critical buckling loads for the SGT, ENET, and Classical Elasticity Theory (CET) by setting $e_0a=0$, $l=0$, and both $e_0a=l=0$, respectively.

4. Results and Discussion

In the present investigation, critical buckling loads (P_1) or (P_{cr}) of the proposed model have been computed by exploiting the Navier approach for HH boundary condition. The critical buckling loads are also calculated for different elasticity theories such as Nonlocal Strain Gradient Theory (NSGT), SGT, ENET, and CET. For the computational purpose, we have considered different parameters from different existing works of literature (Wang, Zhang, Ramesh, & Kitipornchai, 2006) such as $E=1\,TPa$, $G=\frac{E}{2(1+\upsilon)}$, $\upsilon=0.19$, $d=1\,nm$, $I=\frac{\pi d^4}{64}$ and unless mentioned $\frac{L}{d}=10$, and the coefficients of hygrothermal expansion as $\alpha_x=2.1\times10^{-6}\,K^{-1}$ (high-temperature environment) and $\beta_x=0.0026\,(\text{wt.\% of }H_2O)^{-1}$ from Karami, Shahsavari, Janghorban, and Li (2019).

4.1. Validation

The present model is validated by ignoring the microstructure effect and effect of the hygrothermal environment and comparing the critical buckling loads of the system for HH boundary condition with Wang, Zhang, Ramesh, and Kitipornchai (2006). For the computation purpose, all the parameters of the mentioned paper have been retained, and the results exhibit very excellent agreement, which can be observed in Table 1.

Table 1: Validation of the present model with Wang, Zhang, Ramesh, and Kitipornchai (2006).

(e_0a) in nm	P_{cr} by present model				P_{cr} by Wang, Zhang, Ramesh, and Kitipornchai (2006)			
	$\frac{L}{d}=10$	12	14	16	$\frac{L}{d}=10$	12	14	16
0	4.7670	3.3267	2.4514	1.8805	4.7670	3.3267	2.4514	1.8805
0.5	4.654	3.2713	2.4212	1.8626	4.654	3.2713	2.4212	1.8626
1	4.3450	3.1156	2.3348	1.8111	4.3450	3.1156	2.3348	1.8111
1.5	3.9121	2.8865	2.2038	1.7313	3.9121	2.8865	2.2038	1.7313
2	3.4333	2.6172	2.0432	1.6306	3.4333	2.6172	2.0432	1.6306

Table 2: P_{cr} in nN with $\Delta H = 1$ (wt. % of H_2O), and $\frac{L}{d}=10$.

ΔT	NSGT $(e_0a > l)$ $\binom{e_0a=2\,nm}{l=1\,nm}$	NSGT $(l > e_0a)$ $\binom{e_0a=1\,nm}{l=2\,nm}$	SGT $(l = 1\,nm)$	ENET $(e_0a = 1\,nm)$	CET
(a) Linear temperature distribution					
0	1.7258	3.9835	3.1871	2.3030	2.7249
150	1.4784	3.7361	2.9397	2.0556	2.4775
300	1.2310	3.4887	2.6923	1.8082	2.2301
450	0.9836	3.2413	2.4449	1.5608	1.9827
600	0.7362	2.9939	2.1975	1.3134	1.7353
750	0.4888	2.7465	1.9501	1.0660	1.4879
900	0.2414	2.4991	1.7027	0.8186	1.2405
(b) Nonlinear temperature distribution					
0	1.7258	3.9835	3.1871	2.3030	2.7249
150	1.4783	3.7359	2.9396	2.0554	2.4774
300	1.2303	3.4880	2.6916	1.8075	2.2294
450	0.9820	3.2397	2.4433	1.5592	1.9811
600	0.7334	2.9911	2.1947	1.3105	1.7325
750	0.4844	2.7421	1.9457	1.0615	1.4835
900	0.2350	2.4927	1.6963	0.8121	1.2341

4.2. Effect of the thermal environment

This subsection is dedicated to studying the effect of the thermal environment on critical buckling loads of the HH boundary condition. This study is progressed by analyzing the impact of both the linear and nonlinear temperature distributions for NSGT with $(e_0a > l)$, NSGT with $(l > e_0a)$, SGT, ENET, and CET. Furthermore, the high thermal environment is only taken into account. Tabular results of critical buckling loads with linear and nonlinear temperature distributions have been demonstrated in Table 2a and Table 2b, respectively. These results are calculated by considering the change in moisture concentration $(\Delta H) = 1$ (wt. % of H_2O) and all other parameters as mentioned earlier by varying change in temperature from 0 to 900 K with an increment of 150 K. More importantly, this paper ignores the buckling as a result of high temperature. That is why we choose this amplitude for temperature variations. From the tabular results, it is observed that rise in ΔT results in decrease of critical buckling loads for both the linear and nonlinear temperature distribution scenarios for all the elasticity theories. It is also evident that the critical buckling loads for nonlinear temperature distribution are comparatively less than the linear one and this is more prominent in case of high temperatures. Furthermore, a graphical result is also plotted by varying changes in temperature ΔT with $\chi_{\Delta T}$, which is defined as the ratio of critical buckling loads with $\Delta T \neq 0$ and critical buckling loads with $\Delta T = 0$, which is illustrated in Fig. 2. It can be observed that the nanostructures are also physically temperature-dependent and increase of external temperature leads to increase in discrepancy in results of all small-scale theories.

4.3. Effect of hygroscopic environment

In this subsection, we are going to analyze the impact of moisture concentration (ΔH) on the critical buckling loads by taking into account different elasticity theories such as NSGT with $(e_0a > l)$, NSGT with $(l > e_0a)$, SGT, ENET, and CET along with both the linear and nonlinear temperature distribution scenarios. In this regard, tabular results of P_{cr} are presented in Table 3, where Table 3a is the result for the linear case of temperature distribution. At the same time, Table 3b represents the results for the nonlinear distribution of temperature. From these results, it is revealed that the critical buckling loads decrease as the moisture concentration (ΔH) gets larger and it is valid for all the earlier mentioned elasticity theories and both the temperature distribution cases. Physically, it can be interpreted that the moisture concentration into the material can be like some vacancies between molecules and atoms that are filled with water molecules. Naturally, this would lead to weakening the stability and resistance of the structure. Furthermore, nanobeam with linear temperature distribution possesses a higher critical buckling load with respect to the nonlinear case and this is more visible with higher moisture concentration. Additionally, graphical results are also presented in Figs 3 and 4; Fig. 3 illustrates the variation of critical buckling loads with moisture concentration (ΔH) for linear temperature distribution, which is varied from

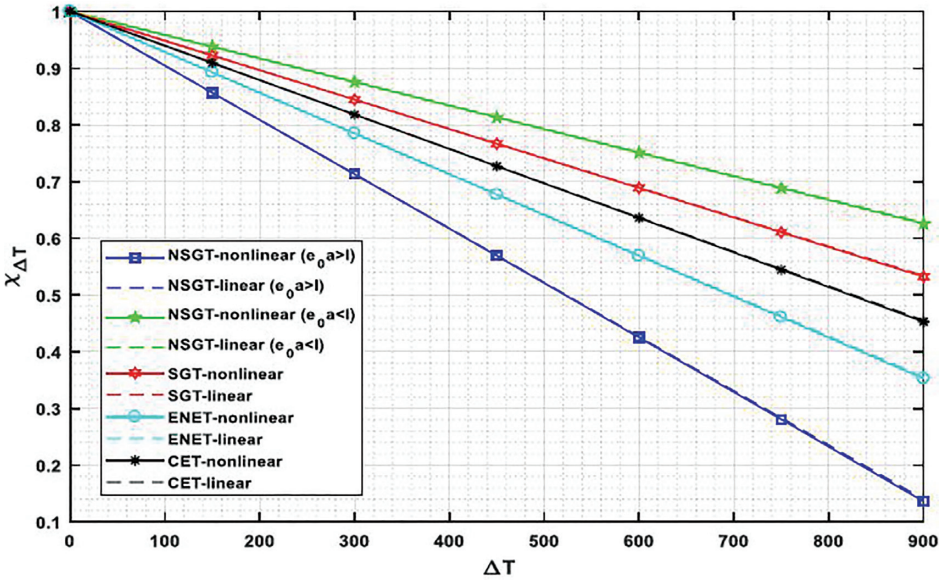

Figure 2: $\chi_{\Delta T}$ versus ΔT for both the linear and nonlinear temperature distributions.

Table 3: P_{cr} in nN with $\Delta T = 1000\,K$, and $\frac{L}{d} = 10$.

ΔH	NSGT $(e_0a > l)$ $\binom{e_0a = 2\,nm}{l = 1\,nm}$	NSGT$(l > e_0a)$ $\binom{e_0a = 1\,nm}{l = 2\,nm}$	SGT $(l = 1\,nm)$	ENET $(e_0a = 1\,nm)$	CET
(a) Linear temperature distribution					
0	2.1185	4.3762	3.5798	2.6957	3.1176
0.25	1.6080	3.8657	3.0693	2.1852	2.6071
0.5	1.0975	3.3552	2.5588	1.6747	2.0966
0.75	0.5870	2.8447	2.0483	1.1642	1.5861
1	0.0765	2.3342	1.5378	0.6536	1.0756
(b) Nonlinear temperature distribution					
0	2.1106	4.3683	3.5719	2.6877	3.1097
0.25	1.6001	3.8578	3.0614	2.1772	2.5992
0.5	1.0896	3.3473	2.5509	1.6667	2.0887
0.75	0.5791	2.8368	2.0404	1.1562	1.5782
1	0.0685	2.3262	1.5299	0.6457	1.0677

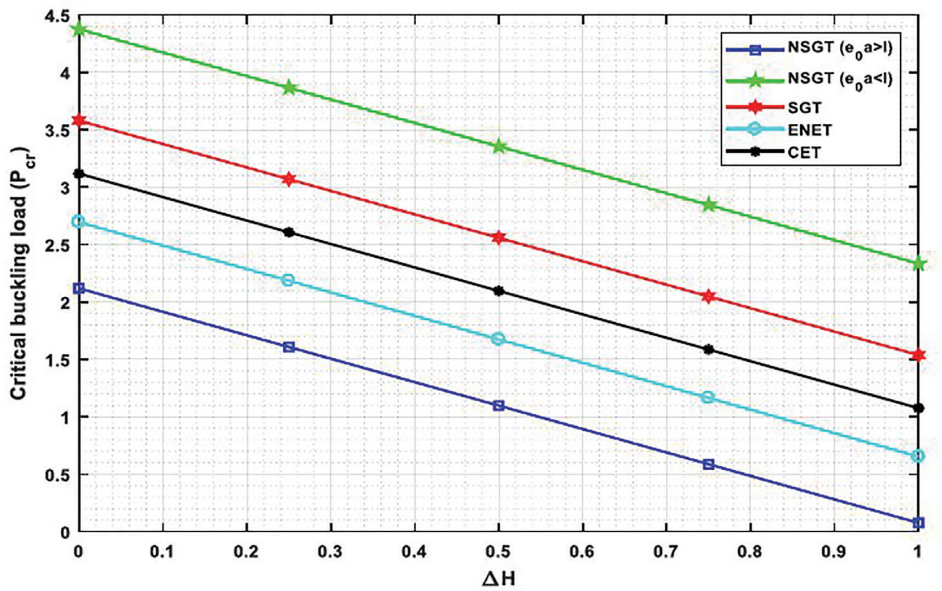

Figure 3: P_{cr} versus ΔH for linear temperature distribution.

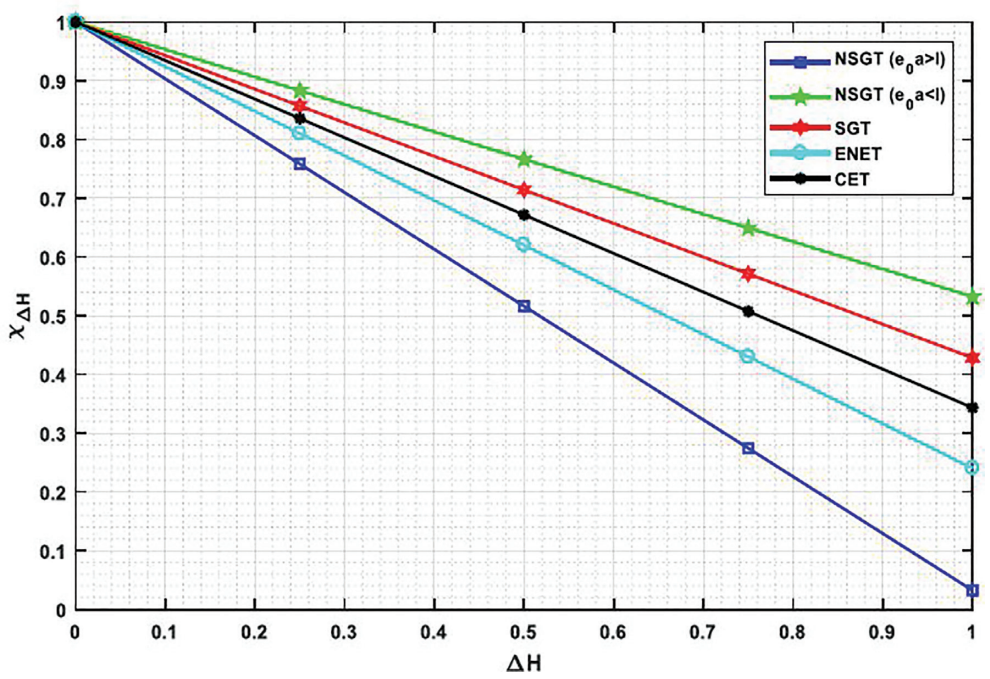

Figure 4: $\chi_{\Delta H}$ versus ΔH for nonlinear temperature distribution.

Table 4: P_{cr} in nN with $\Delta T = 500\,K$ and $\Delta H = 0.5$ (wt. % of H_2O).

L/d	NSGT($e_0a > l$) $\binom{e_0a = 2\,nm}{l = 1\,nm}$	NSGT($l > e_0a$) $\binom{e_0a = 1\,nm}{l = 2\,nm}$	SGT ($l = 1\,nm$)	ENET ($e_0a = 1\,nm$)	CET
(a) Linear temperature distribution					
5	8.2771	30.1304	22.9290	11.4272	16.3462
7.5	3.9864	10.1216	7.9446	5.3051	6.5244
10	1.9222	4.1799	3.3835	2.4993	2.9213
12.5	0.7628	1.7632	1.4146	1.0424	1.2229
15	0.0542	0.5593	0.3851	0.2028	0.2920
(b) Nonlinear temperature distribution					
5	8.2752	30.1284	22.9270	11.4253	16.3442
7.5	3.9844	10.1196	7.9427	5.3031	6.5225
10	1.9202	4.1779	3.3815	2.4973	2.9193
12.5	0.7608	1.7612	1.4126	1.0404	1.2209
15	0.0523	0.5574	0.3831	0.2008	0.2900

0 (wt. % of H_2O) to 1 (wt. % of H_2O) with an increment of 0.25 (wt. % of H_2O). Similarly, Fig. 4 is the graphical result that is plotted with $\chi_{\Delta H}$, which is defined as $\chi_{\Delta H} = \frac{P_{cr} \text{ with } \Delta H \neq 0}{P_{cr} \text{ with } \Delta H = 0}$ and moisture concentration ΔH for nonlinear temperature case.

4.4. Effect of length-to-diameter ratio

Through this subsection, the influence of length-to-diameter ratio (L/d) on critical buckling loads has been investigated by using graphical as well as tabular results, as presented in Table 4 and Figs 5 and 6. Here, rise in temperature $\Delta T = 500\,K$ and moisture concentration $\Delta H = 0.5$ (wt. % of H_2O) have been taken into computation while the length-to-diameter ratio is varied from 5 to 15 with an increase of 2.5. Table 4a demonstrates the tabular results of critical buckling loads for various elasticity theories with linear temperature distribution, whereas Table 4b represents the critical buckling loads for nonlinear temperature distribution. Likewise, Fig. 5 is the variation of critical buckling loads with length-to-diameter ratio for linear temperature case, whereas Fig. 6 is the graphical result plotted by varying $\chi_{\frac{L}{d}}$, which is expressed as $\chi_{\frac{L}{d}} = \frac{P_{cr} \text{ with } L/d \neq 0}{P_{cr} \text{ with } L/d = 5}$ with $\frac{L}{d}$. From all these results, it is very apparent that the critical buckling loads of the nanobeam decrease with increase in $\frac{L}{d}$ and this reduction in critical buckling loads is more visible with the lower value of $\frac{L}{d}$. Also, at a higher value of $\frac{L}{d}$, the difference between the buckling loads of all the elasticity theories becomes less as compared to lower value of $\frac{L}{d}$ and this is valid for both the linear and nonlinear temperature distributions. Likewise, at larger $\frac{L}{d}$ ratio, the nanoscale impact is comparatively unnoticeable for both the linear and nonlinear temperature distributions.

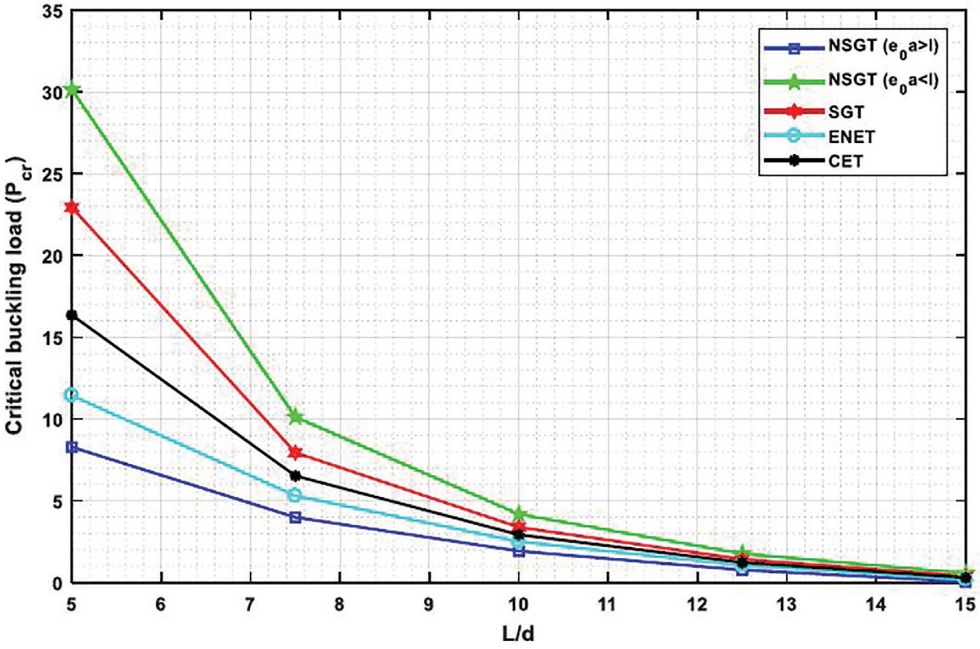

Figure 5: P_{cr} versus L/d for linear temperature distribution.

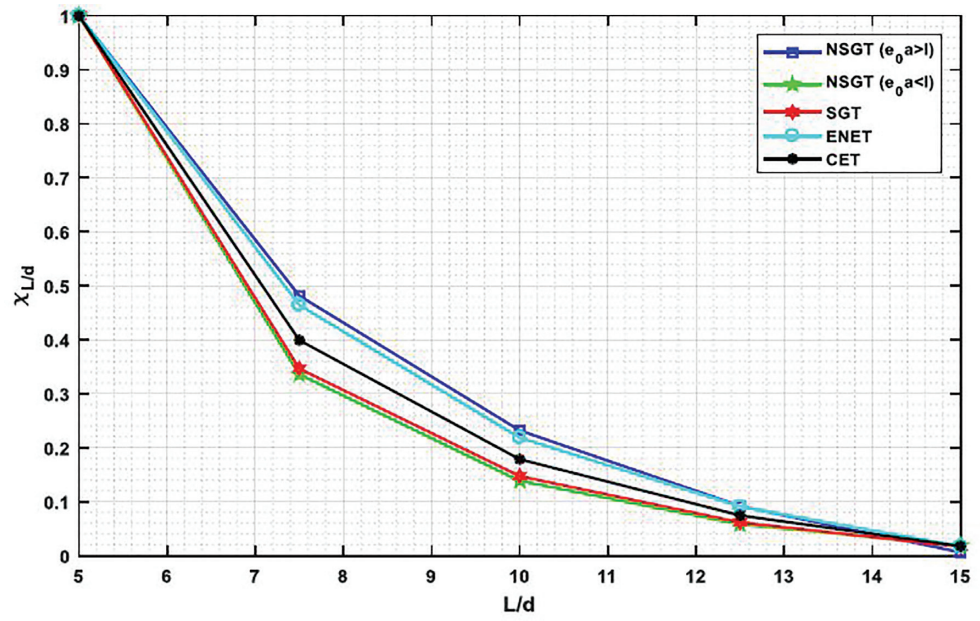

Figure 6: $\chi_{\Delta H}$ versus L/d for nonlinear temperature distribution.

4.5. Effect of the small scale parameter

In this subsection, the impact of small scale parameters (e_0a) on critical buckling loads has been examined, taking into account different elasticity theories such as NSGT, SGT, ENET, and CET along with both the linear temperature distribution (LTD) and nonlinear temperature distribution (NLTD). In this regard, the tabular result is present in Table 5, which are computed with $\Delta T = 500\,K$, $\Delta H = 0.5$ (wt. % of H_2O), and $\frac{L}{d} = 10$. From these results, it is found that P_{cr} decreases as the $e_0a$gets larger, which is applicable for all the abovementioned elasticity theories except SGT, and CET as these two theories don't incorporate nonlocal effects. The graphical results are also presented in Figs 7 and 8, where Fig. 7 illustrates the variation of critical buckling with small scale parameter, which is varied from 0 to 2 nm with an increment of 0.2 nm for linear temperature distribution. Likewise, Fig. 8 demonstrates the variation of χ_{e_0a} (it is defined as the ratio of critical buckling load with small scale effect to without small scale effect) with e_0a.

Table 5: P_{cr} in nN with $\Delta T = 500\,K$, $\Delta H = 0.5$ (wt. % of H_2O), and $\frac{L}{d} = 10$ for both the LTD and NLTD.

e_0a	NSGT ($l = 1\,nm$)		SGT ($l = 1\,nm$)		ENET		CET	
	LTD	NLTD	LTD	NLTD	LTD	NLTD	LTD	NLTD
0	3.3815	3.3815	3.3835	3.3815	2.9213	2.9193	2.9213	2.9193
0.25	3.3520	3.3500	3.3835	3.3815	2.8925	2.8905	2.9213	2.9193
0.5	3.2597	3.2577	3.3835	3.3815	2.8083	2.8063	2.9213	2.9193
0.75	3.1130	3.1111	3.3835	3.3815	2.6744	2.6724	2.9213	2.9193
1	2.9213	2.9193	3.3835	3.3815	2.4993	2.4973	2.9213	2.9193
1.25	2.6955	2.6935	3.3835	3.3815	2.2933	2.2913	2.9213	2.9193
1.5	2.4470	2.4450	3.3835	3.3815	2.0665	2.0645	2.9213	2.9193
1.75	2.1863	2.1843	3.3835	3.3815	1.8285	1.8266	2.9213	2.9193
2	1.9222	1.9202	3.3835	3.3815	1.5876	1.5856	2.9213	2.9193

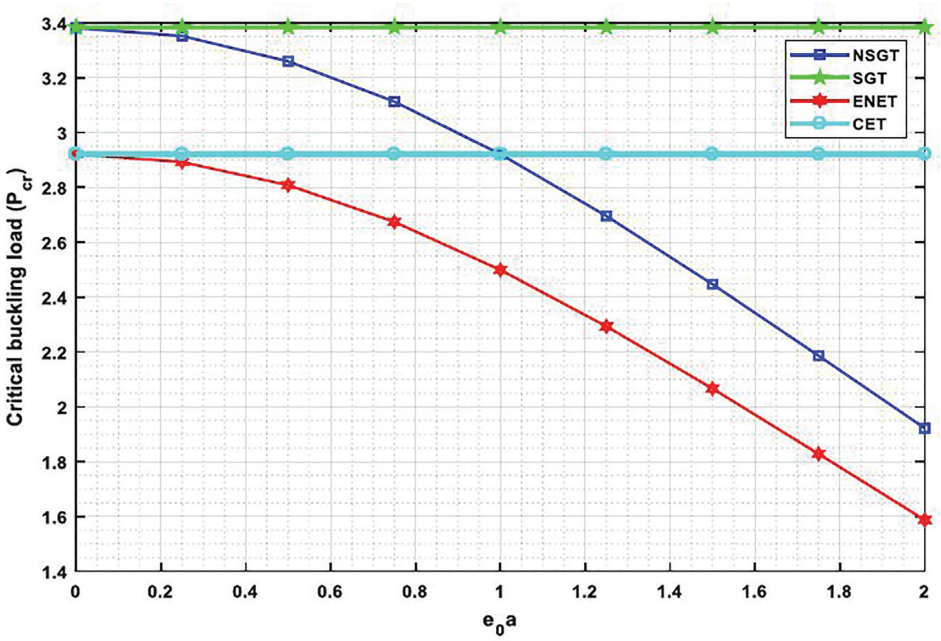

Figure 7: P_{cr} versus e_0a for linear temperature distribution.

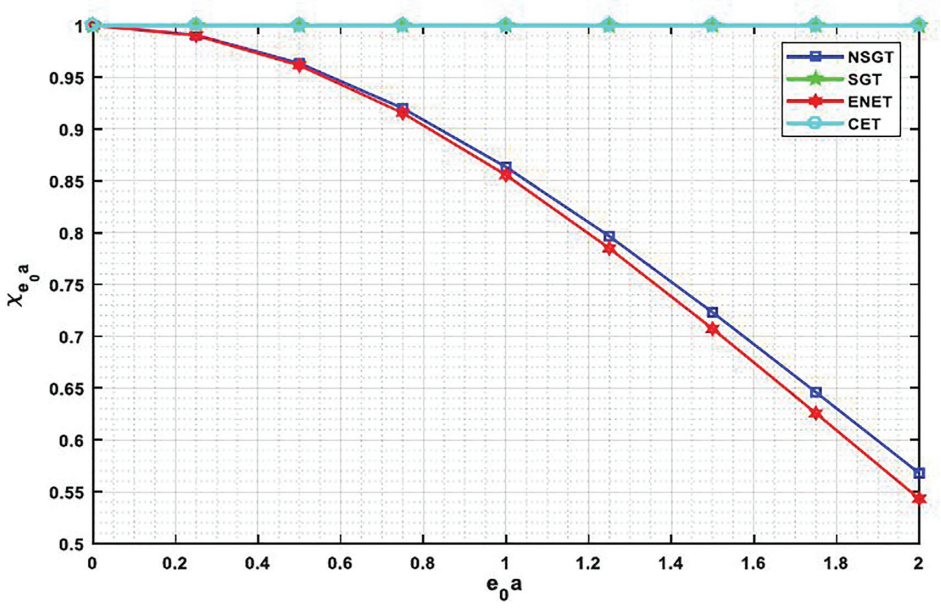

Figure 8: χ_{e_0a} versus e_0a for nonlinear temperature distribution.

Table 6: P_{cr} in nN with $\Delta T = 500\,K$, $\Delta H = 0.5$ (wt. % of H_2O), and $\frac{L}{d} = 10$ for both the LTD and NLTD.

l	NSGT ($e_0a = 1\,nm$)		SGT		ENET ($e_0a = 1\,nm$)		CET	
	LTD	NLTD	LTD	NLTD	LTD	NLTD	LTD	NLTD
0	2.4993	2.4973	2.9213	2.9193	2.4993	2.4973	2.9213	2.9193
0.25	2.5257	2.5238	2.9502	2.9482	2.4993	2.4973	2.9213	2.9193
0.5	2.6049	2.6029	3.0370	3.0350	2.4993	2.4973	2.9213	2.9193
0.75	2.7368	2.7348	3.1815	3.1795	2.4993	2.4973	2.9213	2.9193
1	2.9213	2.9193	3.3835	3.3815	2.4993	2.4973	2.9213	2.9193
1.25	3.1581	3.1561	3.6428	3.6408	2.4993	2.4973	2.9213	2.9193
1.5	3.4470	3.4450	3.9592	3.9572	2.4993	2.4973	2.9213	2.9193
1.75	3.7877	3.7857	4.3322	4.3302	2.4993	2.4973	2.9213	2.9193
2	4.1799	4.1779	4.7613	4.7594	2.4993	2.4973	2.9213	2.9193

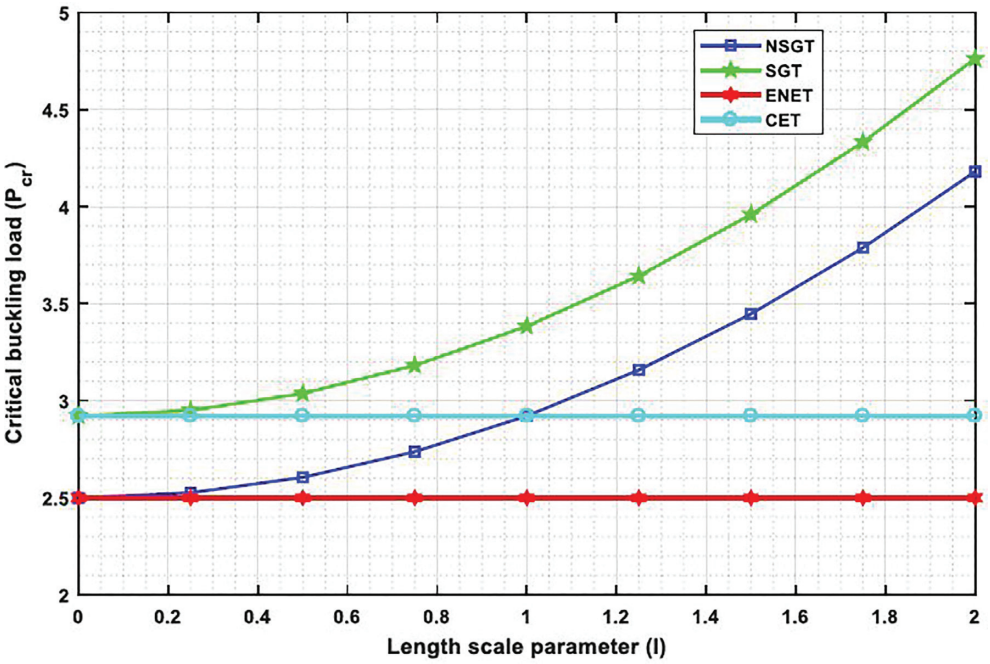

Figure 9: P_{cr} versus l for linear temperature distribution.

4.6. Effect of the length scale parameter

This subsection is aimed to investigate the effect of the length scale parameter (l) on the stability analysis of the proposed model. Various elasticity theories have been taken into consideration in this study, and the results are calculated for different l, which are varied from 0 to 2 nm with an increment of 0.2 nm along with $\Delta T = 500\,K$, $\Delta H = 0.5$ (wt. % of H_2O), and $\frac{L}{d} = 10$ for both the LTD and NLTD. In this regard, Table 6 demonstrates the critical buckling loads with respect to different elasticity theories, i.e. NSGT, SGT, ENET, and CET. Similarly, Fig. 9 represents the variation of P_{cr} with l for linear temperature distribution, and Fig. 10 illustrates the effect of length scale parameter on χ_l, which is expressed as the ratio of critical buckling loads with microstructure effect and without microstructure effect. From these results, it is quite clear that P_{cr} increases with the increase in l for all elasticity theories except ENET and CET as these are not influenced by microstructure effect.

5. Conclusion

In this study, critical buckling loads of the nanobeam, exposed to a hygrothermal environment with nonlinear temperature distribution based on the Murnaghan model, have been computed analytically by exploiting Navier's approach for HH boundary conditions. A parametric study has been carried out to analyze the effects of various scaling parameters considering linear and nonlinear temperature distributions along with different elasticity theories such as NSGT, SGT, ENET, and CET. Following are the main comments:

- With the increase in ΔT, and when considering the higher thermal environment, the critical buckling loads of both the linear and nonlinear temperature distributions for all the elasticity theories decrease. It is also evident that the critical buckling loads

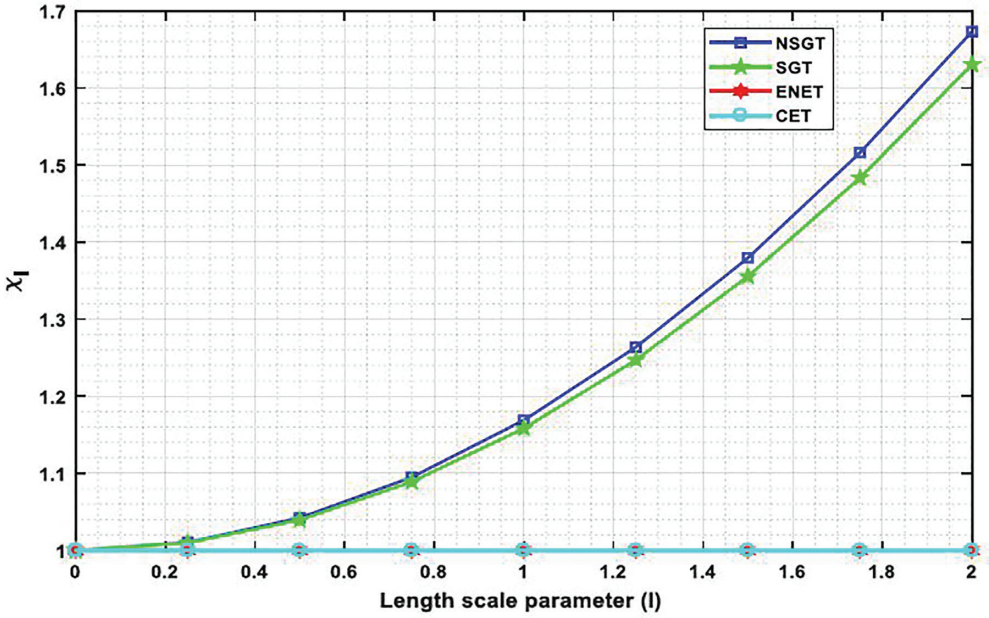

Figure 10: χ_l versus l for nonlinear temperature distribution.

for linear temperature distribution are comparatively higher than the nonlinear one, and this is more prominent in case of high temperatures.

- The critical buckling loads of the nanobeam decrease as the moisture concentration (ΔH) gets higher, and it is valid for all the mentioned elasticity theories and both the temperature distribution scenarios. Furthermore, nanobeam with linear temperature distribution possesses a higher critical buckling load concerning the nonlinear distribution, and this is more visible with higher moisture concentration.
- It is found that the critical buckling loads decrease as the small scale gets larger, which is applicable for all the above elasticity theories except SGT and CET as these two theories do not incorporate nonlocal effects. Similarly, P_{cr} increases with the increase in length scale parameter for all elasticity theories except ENET and CET as these are not influenced by microstructure effect.
- Nanoscale materials can be considered as temperature-dependent along with size-dependent structures. This means external temperature fundamentally affects the nonlocality behavior. It is also observed that with both the temperature distributions, the nanobeam can respond as a hygroscopic-dependent structure.

Acknowledgments

The first two authors are thankful to Defence Research and Development Organisation (DRDO), New Delhi, India (Sanction Code: DG/TM/ERIPR/GIA/17-18/0129/020), for the funding to carry out the present research work.

Conflict of interest statement

None declared.

References

Akgöz, B., & Civalek, Ö. (2017). A size-dependent beam model for stability of axially loaded carbon nanotubes surrounded by Pasternak elastic foundation. *Composite Structures*, *176*, 1028–1038.

Anitescu, C., Atroshchenko, E., Alajlan, N., & Rabczuk, T. (2019). Artificial neural network methods for the solution of second order boundary value problems. *Computers, Materials & Continua*, 59(1), 345–359.

Ansari, R., Sahmani, S., & Rouhi, H. (2011a). Axial buckling analysis of single-walled carbon nanotubes in thermal environments via the Rayleigh–Ritz technique. *Computational Materials Science*, 50(10), 3050–3055.

Ansari, R., Sahmani, S., & Rouhi, H. (2011b). Rayleigh–Ritz axial buckling analysis of single-walled carbon nanotubes with different boundary conditions. *Physics Letters A*, *375*(9), 1255–1263.

Arefi, M., Bidgoli, E. M. R., & Zenkour, A. M. (2018). Size-dependent free vibration and dynamic analyses of a sandwich microbeam based on higher-order sinusoidal shear deformation theory and strain gradient theory. *Smart Structures and Systems*, *22*(1), 27–40.

Arefi, M., & Soltan Arani, A. H. (2018). Higher order shear deformation bending results of a magnetoelectrothermoelastic functionally graded nanobeam in thermal, mechanical, electrical, and magnetic environments. *Mechanics Based Design of Structures and Machines*, *46*(6), 669–692.

Arefi, M., & Zenkour, A. M. (2016). A simplified shear and normal deformations nonlocal theory for bending of functionally graded piezomagnetic sandwich nanobeams in magneto-thermo-electric environment. *Journal of Sandwich Structures & Materials*, *18*(5), 624–651.

Arefi, M., & Zenkour, A. M. (2017a). Transient sinusoidal shear deformation formulation of a size-dependent three-layer piezomagnetic curved nanobeam. *Acta Mechanica*, *228*(10), 3657–3674.

Arefi, M., & Zenkour, A. M. (2017b). Size-dependent vibration and bending analyses of the piezomagnetic three-layer nanobeams. *Applied Physics A*, *123*(3), 202.

Arefi, M., & Zenkour, A. M. (2017c). Transient analysis of a three-layer microbeam subjected to electric potential. *International Journal of Smart and Nano Materials*, *8*(1), 20–40.

Arefi, M., & Zenkour, A. M. (2018a). Free vibration analysis of a three-layered microbeam based on strain gradient theory and three-unknown shear and normal deformation theory. *Steel and Composite Structures*, *26*(4), 421–437.

Arefi, M., & Zenkour, A. M. (2018b). Size-dependent electro-elastic analysis of a sandwich microbeam based on higher-order sinusoidal shear deformation theory and strain gradient theory. *Journal of Intelligent Material Systems and Structures*, *29*(7), 1394–1406.

Arefi, M., & Zenkour, A. M. (2019a). Influence of magneto-electric environments on size-dependent bending results of three-layer piezomagnetic curved nanobeam based on sinusoidal shear deformation theory. *Journal of Sandwich Structures & Materials*, *21*(8), 2751–2778.

Arefi, M., & Zenkour, A. M. (2019b). Influence of micro-length-scale parameters and inhomogeneities on the bending, free vibration and wave propagation analyses of a FG Timoshenko's sandwich piezoelectric microbeam. *Journal of Sandwich Structures & Materials*, *21*(4), 1243–1270.

Barati, M. R., Faleh, N. M., & Zenkour, A. M. (2019). Dynamic response of nanobeams subjected to moving nanoparticles and hygro-thermal environments based on nonlocal strain gradient theory. *Mechanics of Advanced Materials and Structures*, *26*(19), 1661–1669.

Ebrahimi, F., & Barati, M. R. (2017a). Hygrothermal effects on vibration characteristics of viscoelastic FG nanobeams based on nonlocal strain gradient theory. *Composite Structures*, *159*, 433–444.

Ebrahimi, F., & Barati, M. R. (2017b). Small-scale effects on hygro-thermo-mechanical vibration of temperature-dependent nonhomogeneous nanoscale beams. *Mechanics of Advanced Materials and Structures*, *24*(11), 924–936.

Ebrahimi, F., & Salari, E. (2015). Thermal buckling and free vibration analysis of size dependent Timoshenko FG nanobeams in thermal environments. *Composite Structures*, *128*, 363–380.

Eltaher, M. A., Kabeel, A. M., Almitani, K. H., & Abdraboh, A. M. (2018). Static bending and buckling of perforated nonlocal size-dependent nanobeams. *Microsystem Technologies*, *24*(12), 4881–4893.

Fatikow, S., & Rembold, U. (1997). *Microsystem technology and microrobotics*(Vol. *12*). Springer Science & Business Media, Berlin.

Ikeda, K., Kuwayama, H., Kobayashi, T., Watanabe, T., Nishikawa, T., Yoshida, T., & Harada, K. (1990). Silicon pressure sensor integrates resonant strain gauge on diaphragm. *Sensors and Actuators A: Physical*, *21*(1–3), 146–150.

Je̜kot, T. (1996). Nonlinear problems of thermal postbuckling of a beam. *Journal of Thermal Stresses*, *19*(4), 359–367.

Jena, S. K., & Chakraverty, S. (2018). Free vibration analysis of Euler–Bernoulli nanobeam using differential transform method. *International Journal of Computational Materials Science and Engineering*, *7*(3), 1850020.

Jena, S. K., & Chakraverty, S. (2019a). Differential quadrature and differential transformation methods in buckling analysis of nanobeams. *Curved and Layered Structures*, *6*(1), 68–76.

Jena, S. K., & Chakraverty, S. (2019b). Dynamic analysis of single-layered graphene nano-ribbons (SLGNRs) with variable cross-section resting on elastic foundation. *Curved and Layered Structures*, *6*(1), 132–145.

Jena, S. K., & Chakraverty, S. (2019c). Dynamic behavior of an electromagnetic nanobeam using the Haar wavelet method and the higher-order Haar wavelet method. *The European Physical Journal Plus*, *134*(10), 538.

Jena, S. K., Chakraverty, S., & Jena, R. M. (2019). Propagation of uncertainty in free vibration of Euler–Bernoulli nanobeam. *Journal of the Brazilian Society of Mechanical Sciences and Engineering*, *41*(10), 436.

Jena, S. K., Chakraverty, S., Jena, R. M., & Tornabene, F. (2019). A novel fractional nonlocal model and its application in buckling analysis of Euler–Bernoulli nanobeam. *Materials Research Express*, *6*(5), 055016.

Jena, S. K., Chakraverty, S., & Malikan, M. (2019). Implementation of Haar wavelet, higher order Haar wavelet, and differential quadrature methods on buckling response of strain gradient nonlocal beam embedded in an elastic medium. *Engineering with Computers*, 1–14. https://doi.org/10.1007/s00366-019-00883-1.

Jena, S. K., Chakraverty, S., & Malikan, M. (2020a). Implementation of non-probabilistic methods for stability analysis of nonlocal beam with structural uncertainties. *Engineering with Computers*, 1–13. https://doi.org/10.1007/s00366-020-00987-z.

Jena, S. K., Chakraverty, S., & Malikan, M. (2020b). Vibration and buckling characteristics of nonlocal beam placed in a magnetic field embedded in Winkler–Pasternak elastic foundation using a new refined beam theory: an analytical approach. *The European Physical Journal Plus*, *135*(2), 164.

Jena, S. K., Chakraverty, S., & Malikan, M. (2020c). Application of shifted Chebyshev polynomial-based Rayleigh–Ritz method and Navier's technique for vibration analysis of a functionally graded porous beam embedded in Kerr foundation. *Engineering with Computers*, 1–21. https://doi.org/10.1007/s00366-020-01018-7.

Jena, S. K., Chakraverty, S., Malikan, M., & Sedighi, H. M. (2020a). Hygro-magnetic vibration of the single-walled carbon nanotube with nonlinear temperature distribution based on a modified beam theory and nonlocal strain gradient model. *International Journal of Applied Mechanics*, https://doi.org/10.1142/S1758825120500544.

Jena, S. K., Chakraverty, S., Malikan, M., & Sedighi, H. M. (2020b). Implementation of Hermite–Ritz method and Navier's technique for vibration of functionally graded porous nanobeam embedded in Winkler–Pasternak elastic foundation using bi-Helmholtz type of nonlocal elasticity. *Journal of Mechanics of Materials and Structures*, In press.

Jena, S. K., Chakraverty, S., Malikan, M., & Tornabene, F. (2019). Stability analysis of single-walled carbon nanotubes embedded in winkler foundation placed in a thermal environment considering the surface effect using a new refined beam theory. *Mechanics Based Design of Structures and Machines*, 1–15. https://doi.org/10.1080/15397734.2019.1698437.

Jena, S. K., Chakraverty, S., Malikan, M., & Tornabene, F. (2020). Effects of surface energy and surface residual stresses on vibro-thermal analysis of chiral, zigzag, and armchair types of SWCNTs using refined beam theory. *Mechanics Based Design of Structures and Machines*, 1–15. https://doi.org/10.1080/15397734.2020.1754239.

Jena, S. K., Chakraverty, S., & Tornabene, F. (2019a). Buckling behavior of nanobeams placed in electromagnetic field using shifted Chebyshev polynomials-based Rayleigh–Ritz method. *Nanomaterials*, *9*(9), 1326.

Jena, S. K., Chakraverty, S., & Tornabene, F. (2019b). Vibration characteristics of nanobeam with exponentially varying flexural rigidity resting on linearly varying elastic foundation using differential quadrature method. *Materials Research Express*, *6*(8), 085051.

Jena, S. K., Chakraverty, S., & Tornabene, F. (2019c). Dynamical behavior of nanobeam embedded in constant, linear, parabolic, and sinusoidal types of Winkler elastic foundation using first-order nonlocal strain gradient model. *Materials Research Express*, *6*(8), 0850f2.

Jouneghani, F. Z., Dimitri, R., & Tornabene, F. (2018). Structural response of porous FG nanobeams under hygro-thermo-mechanical loadings. *Composites Part B: Engineering*, *152*, 71–78.

Karami, B., Janghorban, M., & Rabczuk, T. (2020). Dynamics of two-dimensional functionally graded tapered Timoshenko nanobeam in thermal environment using nonlocal strain gradient theory. *Composites Part B: Engineering*, *182*, 107622.

Karami, B., Shahsavari, D., Janghorban, M., & Li, L. (2019). Wave dispersion of nanobeams incorporating stretching effect. *Waves in Random and Complex Media*, 1–21. https://doi.org/10.1080/17455030.2019.1607623.

Li, L., & Hu, Y. (2016). Nonlinear bending and free vibration analyses of nonlocal strain gradient beams made of functionally graded material. *International Journal of Engineering Science*, *107*, 77–97.

Lim, C. W., Zhang, G., & Reddy, J. N. (2015). A higher-order nonlocal elasticity and strain gradient theory and its applications in wave propagation. *Journal of the Mechanics and Physics of Solids*, *78*, 298–313.

Lu, L., Guo, X., & Zhao, J. (2017). Size-dependent vibration analysis of nanobeams based on the nonlocal strain gradient theory. *International Journal of Engineering Science*, *116*, 12–24.

Malikan, M., & Nguyen, V. B. (2018). Buckling analysis of piezo-magnetoelectric nanoplates in hygrothermal environment based on a novel one variable plate theory combining with higher-order nonlocal strain gradient theory. *Physica E: Low-dimensional Systems and Nanostructures*, *102*, 8–28.

Malikan, M., Nguyen, V. B., & Tornabene, F. (2018). Damped forced vibration analysis of single-walled carbon nanotubes resting on viscoelastic foundation in thermal environment using nonlocal strain gradient theory. *Engineering Science and Technology, an International Journal*, *21*(4), 778–786.

Malikan, M., Dimitri, R., & Tornabene, F. (2018). Effect of sinusoidal corrugated geometries on the vibrational response of viscoelastic nanoplates. *Applied Sciences*, *8*(9), 1432.

Malikan, M. (2019). On the buckling response of axially pressurized nanotubes based on a novel nonlocal beam theory. *Journal of Applied and Computational Mechanics*, *5*(1), 103–112.

Malikan, M., Dimitri, R., & Tornabene, F. (2019). Transient response of oscillated carbon nanotubes with an internal and external damping. *Composites Part B: Engineering*, *158*, 198–205.

Malikan, M. (2020). On the plastic buckling of curved carbon nanotubes. *Theoretical and Applied Mechanics Letters*, *10*(1), 46–56.

Malikan, M., & Eremeyev, V. A. (2020a). Post-critical buckling of truncated conical carbon nanotubes considering surface effects embedding in a nonlinear Winkler substrate using the Rayleigh–Ritz method. *Materials Research Express*, *7*, 025005.

Malikan, M., & Eremeyev, V. A. (2020b). On the dynamics of a visco–piezo–flexoelectric nanobeam. *Symmetry*, *12*(4), 643.

Malikan, M., Krasheninnikov, M., & Eremeyev, V. A. (2020). Torsional stability capacity of a nano-composite shell based on a nonlocal strain gradient shell model under a three-dimensional magnetic field. *International Journal of Engineering Science*, *148*, 103210.

Mohammadi, M., Safarabadi, M., Rastgoo, A., & Farajpour, A. (2016). Hygro-mechanical vibration analysis of a rotating viscoelastic nanobeam embedded in a visco-Pasternak elastic medium and in a nonlinear thermal environment. *Acta Mechanica*, *227*(8), 2207–2232.

Pradhan, S. C., & Reddy, G. K. (2011). Buckling analysis of single walled carbon nanotube on Winkler foundation using nonlocal elasticity theory and DTM. *Computational Materials Science*, *50*(3), 1052–1056.

Pradhan, S. C. (2012). Nonlocal finite element analysis and small scale effects of CNTs with Timoshenko beam theory. *Finite Elements in Analysis and Design*, *50*, 8–20.

Rabczuk, T., Ren, H., & Zhuang, X. (2019). A nonlocal operator method for partial differential equations with application to electromagnetic waveguide problem. *Computers, Materials & Continua*, *59*(1), 31–55.

Reddy, J. N. (2007). Nonlocal theories for bending, buckling and vibration of beams. *International Journal of Engineering Science*, *45*(2–8), 288–307.

Roque, C. M. C., Ferreira, A. J. M., & Reddy, J. N. (2011). Analysis of Timoshenko nanobeams with a nonlocal formulation and meshless method. *International Journal of Engineering Science*, *49*(9), 976–984.

Samaniego, E., Anitescu, C., Goswami, S., Nguyen-Thanh, V. M., Guo, H., Hamdia, K., Zhuang, X., & Rabczukab, T. (2020). An energy approach to the solution of partial differential equations in computational mechanics via machine learning: concepts, implementation and applications. *Computer Methods in Applied Mechanics and Engineering*, *362*, 112790.

Sedighi, H. M., & Malikan, M. (2020). Stress-driven nonlocal elasticity for nonlinear vibration characteristics of carbon/boron-nitride hetero-nanotube subject to magneto-thermal environment. *Physica Scripta*, *95*(5), 055218.

Sedighi, H. M., Ouakad, H. M., Dimitri, R., & Tornabene, F. (2020). Stress-driven nonlocal elasticity for the instability analysis of fluid-conveying C-BN hybrid-nanotube in a magneto-thermal environment. *Physica Scripta*, *95*(6), 065204.

Senthilkumar, V. (2020). Flexural wave dispersion of nonlocal bi-Helmholtz-type stress gradient theory. *Mathematics and Mechanics of Solids*, https://doi.org/10.1177/1081286519897300.

She, G. L., Yuan, F. G., Ren, Y. R., & Xiao, W. S. (2017). On buckling and postbuckling behavior of nanotubes. *International Journal of Engineering Science*, *121*, 130–142.

She, G. L., Jiang, X. Y., & Karami, B. (2019). On thermal snap-buckling of FG curved nanobeams. *Materials Research Express*, *6*(11), 115008.

Takahashi, S. (2018). Measurement of third-order elastic constants and stress dependent coefficients for steels. *Mechanics of Advanced Materials and Modern Processes*, *4*(1), 2.

Vinyas, M., Harursampath, D., & Kattimani, S. C. (2020). On vibration analysis of functionally graded carbon nanotube reinforced magneto-electro-elastic plates with different electro-magnetic conditions using higher order finite element methods. *Defence Technology*, https://doi.org/10.1016/j.dt.2020.03.012

Vu-Bac, N., Lahmer, T., Zhuang, X., Nguyen-Thoi, T., & Rabczuk, T. (2016). A software framework for probabilistic sensitivity analysis for computationally expensive models. *Advances in Engineering Software*, *100*, 19–31.

Wang, C. M., Zhang, Y. Y., Ramesh, S. S., & Kitipornchai, S. (2006). Buckling analysis of micro-and nano-rods/tubes based on nonlocal Timoshenko beam theory. *Journal of Physics D: Applied Physics*, *39*(17), 3904.

Zhen, Y., & Fang, B. (2010). Thermal–mechanical and nonlocal elastic vibration of single-walled carbon nanotubes conveying fluid. *Computational Materials Science*, *49*(2), 276–282.